Journal of Molecular Catalysis A: Chemical 340 (2011) 65–76

Contents lists available at ScienceDirect

Journal of Molecular Catalysis A: Chemical

journal homepage: www.elsevier.com/locate/molcata

Preparation of MoO_3/SiO_2–Al_2O_3 metathesis catalysts via wet impregnation with different Mo precursors

Damien P. Debecker[a,*], Mariana Stoyanova[b], Uwe Rodemerck[b], Eric M. Gaigneaux[a]

[a] Institute of Condensed Matter and Nanosciences - MOlecules, Solids and reactiviTy (IMCN/MOST), Université catholique de Louvain, Croix du Sud 2/17, 1348 Louvain-La-Neuve, Belgium[1]

[b] Leibniz-Institut für Katalyse e.V. an der Universität Rostock, Albert-Einstein-Str. 29a, 18059 Rostock, Germany

ARTICLE INFO

Article history:
Received 6 January 2011
Received in revised form 15 March 2011
Accepted 16 March 2011
Available online 31 March 2011

Keywords:
Propylene
Alkene metathesis
Anderson-type alumino heteropolymolybdate
Peroxopolymolybdate
Alumino-silicate

ABSTRACT

Molybdenum oxide supported on mesoporous silica–alumina is an efficient catalyst for the light olefins metathesis. Preparation via the classical wet impregnation with ammonium heptamolybdate (AHM) suffers from several downsides related to the control of the species formed on the surface and the build up of inactive species (MoO_3 crystals and $Al_2(MoO_4)_3$). This study explores the synthesis, properties and propene metathesis activity of MoO_3/SiO_2–Al_2O_3 catalysts prepared with two Mo precursors chosen as alternatives to AHM. Characterization is done on the precursor solutions, on the dried catalyst precursors and on the calcined catalysts (ICP-AES, N_2-physisorption, XRD, Raman spectroscopy, XPS and ^{27}Al MAS NMR). Firstly, oxalic acid is used as an additive with the objective to perturb the Mo speciation in the AHM impregnation solution. It affects the catalysts texture and impedes the formation of $Al_2(MoO_4)_3$. Samples are totally amorphous and outcompete the reference samples prepared with AHM. Secondly, a molybdenum oxide hydrates solution is used as impregnation solution. The MoO_3 phase formed is also totally amorphous, the texture is preserved, the spreading of the Mo phase is enhanced and the activity is high. However, at high Mo loading the build-up of $Al_2(MoO_4)_3$ provokes a decrease in activity.

1. Introduction

Olefin metathesis is a crucial reaction for the petrochemical industry [1–6], which allows regulating the stocks of light alkenes as a function of the market demand. This reaction can be carried out with tungsten [7,8], molybdenum [9,10] or rhenium [11,12] oxides supported on high specific surface area silica, alumina or silica–alumina. MoO_3-based metathesis catalysts, being relatively active and robust, are considered with a lot of interest. Current research efforts are mainly devoted to the development of improved preparation methods which ensure the stabilization of active Mo oxide species on the surface. In this perspective, several innovative preparation methods proved successful in the development of active MoO_3-based metathesis catalysts (e.g. thermal spreading [13–16], non-hydrolytic sol–gel [17], flame spray pyrolysis [18]). As a rule, increased performances are obtained when the preparation allows the stabilization of highly dispersed species. Efforts are made also to understand the impact of the support composition and structure [19–23]. Theoretical studies are devoted to the understanding of the nature of the metathesis active centres which experimentally remain poorly described [22,24,25]. Some authors also address the issue of catalyst deactivation [26,27] and study the most favourable way to run the activation of the catalysts [28].

In a previous work, we have reported on the preparation of MoO_3/SiO_2–Al_2O_3 metathesis catalysts by conventional wet impregnation of ammonium heptamolybdate (AHM) on a commercial silica–alumina support [9]. The aim was to identify the parameters that dictate the metathesis activity of such systems. In a search for higher metathesis activity, the increase of the Mo loading and calcination temperature proved to be profitable only to a limited extent. The performance of the catalysts level off due to the build-up of bulk MoO_3 crystals and of aluminium molybdate. The formation of the latter species appeared clearly linked to the preparation method and particularly to the nature of the Mo precursor used. The heptamolybdate anions present in the impregnation solution proved to interact strongly with the external surface of the support, resulting in an uneven dispersion of the Mo phase. In addition the heptamolybdate clusters were thought to play the role of nucleation points for the sintering toward MoO_3 crystals. Also, the wet step resulted in the formation of mixed aluminium–molybdenum species ($[Al(OH)_6Mo_6O_{18}]^{3-}$). This Anderson-type heteropolyanion, seems to play a role in the

* Corresponding author. Tel.: +32 10473665; fax: +32 10473649.
E-mail addresses: damien.debecker@uclouvain.be (D.P. Debecker), eric.gaigneaux@uclouvain.be (E.M. Gaigneaux).

[1] *Note*: IMCN and MOST are new research entities involving the group formerly known as "Unité de catalyse et chimie des matériaux divisés".

1381-1169/$ – see front matter © 2011 Elsevier B.V. All rights reserved.
doi:10.1016/j.molcata.2011.03.011

accumulation of MoO_3 crystals and of $Al_2(MoO_4)_3$ during the calcination step.

Bearing these limitations in mind, our present strategy is an attempt to improve the dispersion of the Mo oxide phase at the surface of the support. To that end, the nature of the precursor used in the impregnation step was changed.

The dissolution of the ammonium heptamolybdate salt in water leads to $Mo_7O_{24}^{6-}$ species in solution, in complex equilibrium with other species [29]. Breaking the heptamolybdate clusters to form monomeric or at least smaller molybdate species in solution could possibly lead to a better spreading of the MoO_3 phase created at the surface of the support. Beltràn et al. reported that molybdenum oxalate forms stable dimeric and monomeric complexes in aqueous solution [30]. Such species could have a lower tendency to agglomerate and generate bulky MoO_3 crystals. Our strategy is also supported by earlier studies that showed how the addition of oxalic acid influences the morphology of a MoO_3 phase formed at the surface of a silica powder [31] or at the surface of Si wafers [32]. It was suggested that the heptamolybdate cluster is broken and that oxalate ions stabilize smaller Mo complexes in solution. Complexing agents like oxalic acid or citric acid, are often used to prepare Mo-based catalysts [31,33–38]. The organic ligands can possibly alter the interaction between the support and the oxomolybdenum species. For example, while the heptamolybdate anion tends to interact strongly with the external surface of alumina extrudates, Weckhuysen et al. have successfully used citric acid as a complexing agent to lower this interaction and ensure a homogeneous distribution of the Mo phase inside the porosity of the carrier [29].

With the same aim of improving the Mo active phase dispersion, a second strategy was imagined. The idea is to use a Mo precursor which could be decomposed at lower calcination temperature. Lower temperature treatment might satisfactorily reduce the tendency of Mo oxide to sinter. The preparation of a "peroxopolymolybdate" solution was performed following the method of Kudo. This method involves the use of hydrogen peroxide to oxidize metallic Mo [39,40]. The species formed in solution can be described by the following general formula: $MoO_3{\cdot}nH_2O{\cdot}mH_2O_2$. Upon catalytic removal of the peroxide species in excess, the yellow solution is composed of molybdenum hydrates [41]. The group of Brégault highlighted the quality of this kind of precursors for the production of highly dispersed MoO_x by impregnation on silica [42–44]. It is noteworthy that only water and possibly residual hydrogen peroxide moieties must be removed from the catalyst to obtain the desired MoO_3 phase. No ammonium moieties or organic ligands need to be thermally decomposed.

2. Experimental

2.1. Catalysts preparation

All catalysts were prepared by the wet impregnation of a commercial silica–alumina support (Aldrich, Grade 135). The support contains ca. 13 wt.% of Al_2O_3 and has a specific surface area of 490 $m^2\,g^{-1}$. Prior to impregnation, the support was calcined at 500 °C for 15 h under static air.

Reference catalysts were prepared from a solution of ammonium heptamolybdate, as described in [9,20]. $(NH_4)_6Mo_7O_{24}{\cdot}4H_2O$, Aldrich, had a purity of 99.98%. An initial precursor solution was prepared by dissolution of 12.268 g AHM in distilled water (6.66 g Mo per litre). An appropriate amount of this precursor solution (depending on the nominal MoO_3 loading targeted for each synthesis) was diluted in distilled water to yield a 200 ml impregnation solution. 4 g of calcined support was then suspended in the impregnation solution for 2 h under magnetic stirring. Water was then evaporated under reduced pressure in a rotavapor at 40 °C. The recovered solid was dried at 110 °C for one night and calcined for 2 h in a muffle furnace under static air. The samples are denoted AHM*xy*, where 'AHM' stands for the ammonium heptamolybdate precursor, '*x*' is the nominal MoO_3 weight loading (%) and '*y*' is the calcination temperature (°C).

Oxalic acid was added to a second solution of AHM (6.66 g of Mo per litre). The amount of oxalic acid is calculated in order to reach three moles of acid for one mole of Mo. Then the same wet impregnation, drying and calcination procedures were used. The catalysts are denoted OXA*x* where 'OXA' stand for the impregnation in the presence of oxalic acid and where '*x*' is the nominal MoO_3 weight loading (%). These catalysts were calcined at 400 °C.

A solution of molybdenum hydrates was prepared from metallic molybdenum (99.95%, Alfa Aesar) and a 15% w/w solution of hydrogen peroxide (obtained from the dilution of a 30% w/w solution from Aldrich, semiconductor grade). 2 g of metallic molybdenum powder was added progressively to 30 ml of the hydrogen peroxide solution. The mixture was kept at 0 °C in an ice bath. After effervescence had ended, a platinum grid was placed into the solution in order to catalyse the decomposition of excess hydrogen peroxide. The solution was finally filtered and diluted to the desired concentration (depending on the targeted loading) and used as impregnation solution (200 ml) as described above. Drying and calcination procedures are also identical. The catalysts are denoted MoH*xy*, where 'MoH' stands for the molybdenum hydrates precursor, '*x*' is the nominal MoO_3 weight loading (%) and '*y*' is the calcination temperature (°C).

2.2. Catalyst characterization

The weight percentages of Mo, Si and Al were measured by Inductively Coupled Plasma-Atomic Emission Spectroscopy (ICP-AES) on an Iris Advantage apparatus from Jarrell Ash Corporation. The materials were dried at 105 °C prior to measurements. One experiment was also carried out on the impregnation juice. The latter is abbreviated "IJ" and defined as the impregnation solution at the end of the impregnation procedure. In this test, the wet impregnation procedures were repeated as to prepare one AHM10, one OXA10 and one MoH10 catalyst. At the end of the 2 h stirring step, the suspension was allowed to rest for exactly 10 min during which sedimentation of the solid at the bottom of the flask occurred. Then 1 ml of the liquid phase (IJ) was collected with a pipette and the amount of Mo, Si and Al in solution was analyzed by ICP-AES. Also one blank impregnation was realized using water as impregnation solution and the impregnation juice was also analyzed after 2 h stirring and 10 min rest.

N_2 physisorption experiments were performed at −196 °C on a Micromeritics Tristar. The samples were outgassed at 150 °C under vacuum (2 Pa). The specific surface area was determined via the BET method in 0.05–0.30P/P_0 range. The pore size distribution was derived from the desorption branch using the BJH method. The average pore diameter is calculated as (4 × Pore Volume/BET specific surface area).

X-ray diffraction (XRD) measurements were performed with a Siemens D5000 diffractometer using the Kα radiation of Cu (λ = 1.5418 Å). The 2θ range was recorded between 5° and 75° at a rate of 0.02° s^{-1}. The ICDD-JCPDS database was used to identify the crystalline phases.

Confocal Raman spectroscopy was done on the InVia Raman microscope (Renishaw) equipped with a diode light (785 nm). The resolution was set to 4 cm^{-1}. Acquisition time was 10 s and 10 scans were recorded and averaged for each catalyst. The laser power was set to 10 mW and the 50× objective was used. The precursor solution was analyzed via Fourier transform Raman spectroscopy (FT-Raman) with the Bruker RFS 100/S apparatus. About 1 ml of the

solution was introduced in a dedicated quartz cell. A coherent Nd-YAG laser of 1064 nm wavelength was used and its power was set to 450 mW. The resolution was 4 cm^{-1} and the frequency was analyzed in the 1600–100 cm^{-1} range. For each reported spectra 720 scans were recorded and averaged.

X-ray photoelectron spectroscopy (XPS) was performed on a Kratos Axis Ultra spectrometer (Kratos Analytical, Manchester, UK) equipped with a monochromatized aluminium X-ray source (powered at 10 mA and 15 kV). The pressure in the analysis chamber was about 10^{-6} Pa. The analyzed area was 700 μm × 300 μm. The pass energy of the hemispherical analyzer was set at 160 eV for the wide scan and 40 eV for narrow scans. Charge stabilization was achieved by using the Kratos Axis device. The electron source was operated at 1.8 A filament current and a bias of −1.1 eV. The charge balance plate was set at −2.8 V. The sample powders were pressed into small stainless steel troughs mounted on a multi specimen holder. The following sequence of spectra was recorded: survey spectrum, C 1s, O 1s, Si 2p, Al 2p, Mo 3d, Mo 3p and N 1s and C 1s again to check for charge stability as a function of time and for the absence of degradation of the sample during the analyses. The binding energy (BE) values were referred to the C–(C, H) contribution of the C 1s peak fixed at 284.8 eV. Molar fractions (%) were calculated using peak areas normalized on the basis of acquisition parameters after a linear background subtraction, with experimental sensitivity factors and transmission factors provided by the manufacturer.

The Bruker Avance 500 apparatus was used to record the magic angle spinning nuclear magnetic resonance (MAS-NMR) of ^{27}Al, using a flip of 10° (with respect to the vertical) and recording 5000 scans for each sample at intervals of 0.1 s. The sample rotation speed was 15,000 rpm.

2.3. Propene metathesis

The evaluation of the catalysts metathesis activity was carried out in a multi-channel apparatus with a capacity of treating of up to 15 samples under identical conditions [45]. The whole design allows fully automated control of gas flows and of three temperature zones (gas pre-heating, reactor, and post-reactor lines with 16-port valve) along with reactor switching and product sampling. The catalysts (200 mg) in the 200–315 μm particle size range were placed in quartz straight reactors (5 mm i.d.). In each experiment, several samples were pre-treated in parallel by heating up to 550 °C with temperature ramp of 5 K min^{-1} in N_2 (14 ml min^{-1} flow in each reactor) and kept at this temperature for 2 h. Afterwards the system was cooled down to the reaction temperature (40 °C) under the same N_2 flow. A propene (AirLiquide, 99.95% purity) flow of 8 ml min^{-1} was admitted for 1 h sequentially in each reactor in order to measure the initial metathesis activity of each sample. During activity measurement in the selected reactor at atmospheric pressure, the other reactors are kept under N_2 flow. Propene and nitrogen were purified over Molsieve 3A (Roth) filters. N_2 was additionally purified over an oxygen filter (Oxysorb-glass, Linde). The composition of the reaction gas was analyzed by an Agilent 6890 GC. Product analysis took about 6.5 min for each injection. Eight by-pass analyses of the educt gas were averaged as a basis for calculating the conversion. The separation of hydrocarbons was performed on a HP-AL/M column (30 m length, 0.53 mm i.d., 0.15 μm film thickness) applying a temperature ramp between 90 and 140 °C and FID detection.

The selectivity to metathesis products was always found to be very close to 100% (typically 99%). Only traces of secondary metathesis products (1-butene, pentenes, hexenes) and isomerization products (isobutene) were detected. The specific activity is calculated on the basis of metathesis products (ethene and *trans*- and *cis*-butene) formation. It is defined as the number of moles of propene converted to metathesis products per gram of catalyst and per hour. The standard deviation for activity measurements is less than 3% in relative.

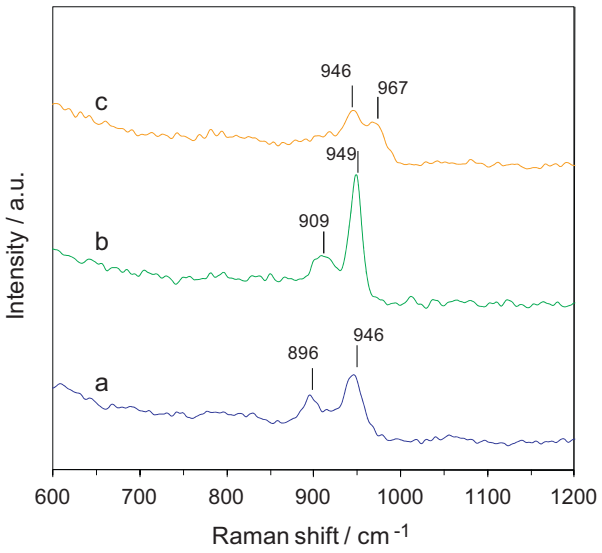

Fig. 1. FT Raman spectrum of (a) an aqueous solution of ammonium heptamolybdate (6.66 g of Mo per litre; pH = 5.4), (b) the OXA precursor solution (6.66 g of Mo per litre; pH = 1.8) and (c) the MoH precursor solution (8 g of Mo per litre; pH = 2.0).

3. Results and discussions

The catalysts obtained via impregnation of AHM have been thoroughly characterized and tested in the metathesis of propene, as published in reference [9]. In the present paper, the OXA and MoH systems will be described sequentially and results will be compared to the AHM catalysts, taken as reference systems.

3.1. Ammonium heptamolybdate with oxalic acid (OXA)

3.1.1. Catalysts characterization

The initial precursor solution ('OXA') was obtained by dissolving AHM into water and adding oxalic acid as to have three moles of acid for one mole of Mo. The pH of this solution was 1.8. Fig. 1 shows the Raman spectrum of this impregnation solution. Two bands are detected, close to the usual signals of heptamolybdate, at 950 and 911 cm^{-1} [9,29].

Table 1 includes the experimental MoO_3 weight loading and the textural properties of the OXA catalysts. The MoO_3 loading of these catalysts was varied in the 5–19 wt.% range. The experimental weight loading corresponds well to the nominal loading. These samples were all calcined at 400 °C. Analysis of their texture shows that the specific surface area roughly tends to decrease with increasing loading (Table 1). So does the pore volume. The average pore diameter is significantly lower than in the support.

Fig. 2 shows how the impregnation of the support using AHM-oxalate precursor has affected the pore size distribution of the support. For all catalysts a clear downward shift (with respect to the Y axis) is observed. This correlates with the marked decrease in the pore volume (Table 1). At high Mo loading the shape of the curve is changed. The amount of large mesopores decreases, while small pores around 2–3 nm come up.

X-ray diffraction analysis of the OXA samples reveals only the broad band related to the amorphous support (supplementary information Fig. S1). Even at the highest MoO_3 loading, no crystals are detected.

The detection limit of XRD for MoO_3 crystals lays around 5-nm sized crystallites [46,47]. In order to go further in the description

Table 1
Textural properties (N_2-physisorption) and experimental MoO_3 weight loading (ICP-AES) of the OXA catalysts.

Name	Calcination temperature (°C)	MoO_3 loading (wt.%)	SSA ($m^2\,g^{-1}$)	Pore volume ($ml\,g^{-1}$)	Pore diameter (nm)
Support	500	–	490	0.71	5.8
OXA5	400	4.5	440	0.56	5.1
OXA10	400	9.6	470	0.51	4.3
OXA13	400	13.3	410	0.44	4.3
OXA19	400	19.2	310	0.37	4.7

of the MoO_x species, Raman spectroscopy was carried out (Fig. 3). Such analysis is delicate in the present case because of the intense fluorescence background of the support [9]. On the other hand, MoO_3 crystals – even very small crystallites – are strong Raman scatterer and are readily detected if present [14,15]. Here, no bands related to crystalline MoO_3 were detected. This confirms XRD analysis concerning the absence of MoO_3 crystals and goes further by demonstrating the absence of even small MoO_3 crystallites. Only one large band is detected around 950 cm^{-1}, attributed to the terminal ν(Mo=O) vibration of surface polymolybdates [46,48–50]. This band increases with increasing MoO_3 loading. It is relatively broad, which can be taken as an indication of the interaction between molybdenum oxide species and the support [46].

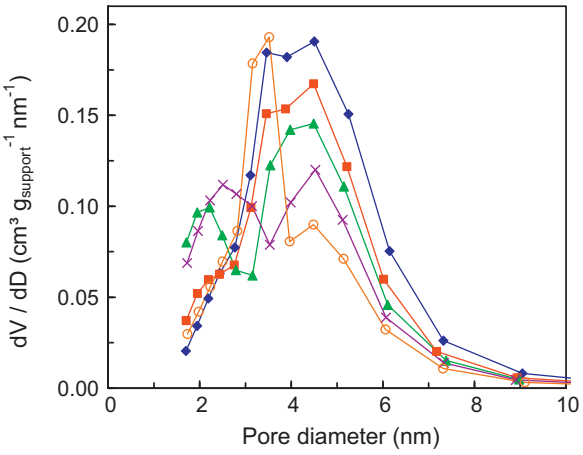

Fig. 2. Pore size distribution as measured by the BJH method on the desorption isotherms of (♦) the support, (■) OXA5, (▲) OXA10, (×) OXA13 and (○) OXA19.

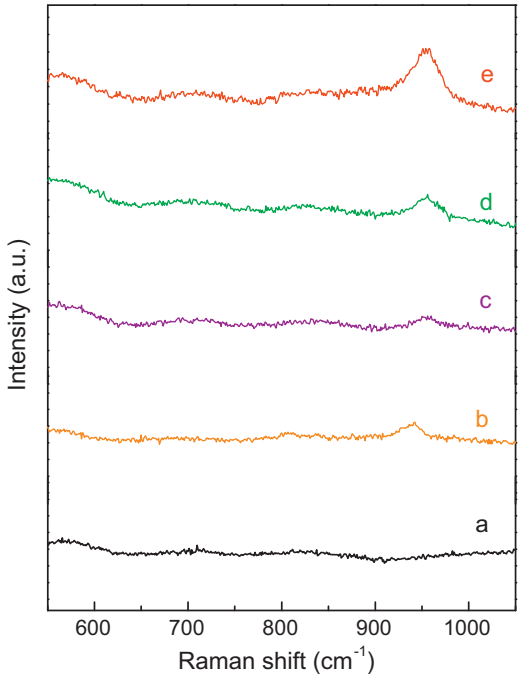

Fig. 3. Raman spectra of (a) the SiO_2–Al_2O_3 support, (b) OXA5, (c) OXA10, (d) OXA13 and (e) OXA19.

The catalysts surface composition was determined by XPS. From this, the surface Mo/(Si + Al) atomic ratio was calculated and compared to the bulk Mo/(Si + Al) atomic ratio. The latter is calculated from the experimental bulk composition of each sample (determined by ICP-AES). In Fig. 4, the surface ratio is plotted against the bulk ratio which provides insights on the location of the Mo phase with respect to the silica–alumina support. Bulk and surface Mo/(Si + Al) atomic ratios would be equal for a totally homogeneous sample (dotted line in Fig. 4). It turns out that the amount of Mo at the surface of OXA catalysts tends to be lower than in the bulk.

The ^{27}Al MAS-NMR spectrum of the bare support is composed of three bands around 2, 30 and 54 ppm (Fig. 5). The signal around 54 ppm is attributed to tetrahedrally coordinated framework Al atoms (Al_{TET}) typically found in silico-aluminic materials [51]. The signal at about 2 ppm corresponds to Al octahedrally coordinated (Al_{OCT}). It is attributed either to γ-Al_2O_3 [52] or to an amorphous polymeric aluminium oxide phase [53]. The intermediate band at 30 ppm is attributable to five-coordinated Al atoms [51,54].

The environment of the Al atoms present in the silica–alumina support is drastically affected by the impregnation with the 'OXA' solution (Fig. 5). In the 10%-loaded sample, analyzed by MAS-NMR after drying (uncalcined), the Al_{TET} and Al_{PEN} species disappear almost completely. Interestingly, no band attributable to the interaction of extracted Al with Mo atoms is detected. This contrasts with the situation encountered with catalysts prepared via standard impregnation of AHM, for which the $[Al(OH)_6Mo_6O_{18}]^{3-}$

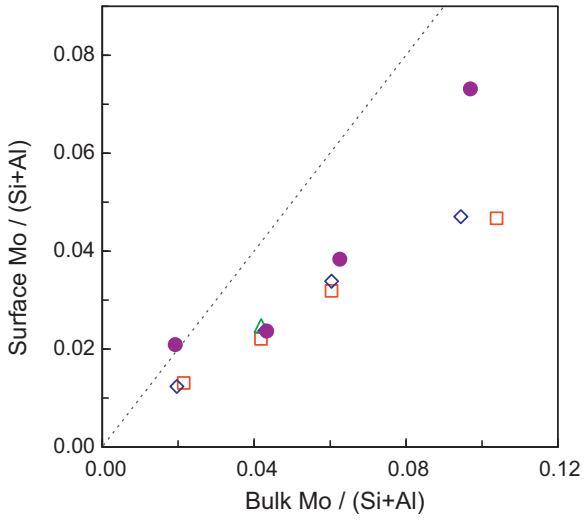

Fig. 4. Mo/(Si + Al) atomic ratio determined via XPS as a function of the bulk Mo/(Si + Al) ratio for (●) OXAx, (Δ) MoHx300, (□) MoHx400 and (◊) MoHx500 catalysts. The dotted line represents the value expected for totally homogeneous samples (same amount of Mo at the surface and in the bulk). *Note*: the bulk ratios are calculated from the experimental composition determined by ICP-AES.

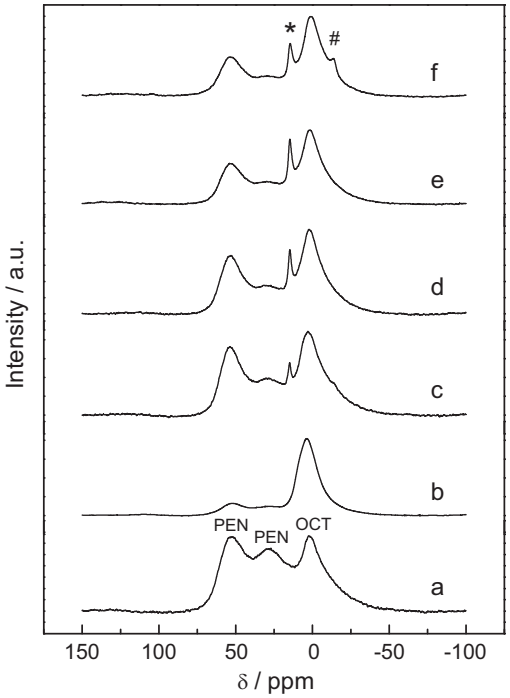

Fig. 5. ^{27}Al MAS-NMR spectra of (a) the support, (b) OXA10 dried but not calcined, (c) OXA5, (d) OXA10, (e) OXA13 and (f) OXA19. The Al_{TET}, Al_{PEN} and Al_{OCT} broad signals are indicated on the first spectrum. [$AlMo_6$] and $Al_2(MoO_4)_3$ are marked with "*" and "#" respectively.

species (hereafter abbreviated [$AlMo_6$]) were detected in significant amounts after impregnation [9]. In calcined OXA catalysts, the Al_{TET} (ca. 54 ppm) signal is almost restored while the Al_{PEN} (ca. 30 ppm) increases but remains lower than in the fresh support. [$AlMo_6$] is detected on calcined catalysts at 15 ppm. In the catalyst with the highest loading (OXA19), a small peak at −14 ppm reveals also the presence of $Al_2(MoO_4)_3$.

To gain further insight in the phenomena that occur during the impregnation step, an ICP-AES analysis was conducted on the impregnation juice. First, the Al/Si ratio was determined for the fresh support (solid sample). Then the blank impregnation juice was analyzed (same impregnation procedure but without Mo precursor). As small particles of support remained in suspension when the liquid was sampled, Si and Al were detected in the liquid sample. As expected, the Al/Si ratio is close to the one of the solid (Fig. 6). In contrast, stirring the silica–alumina support in the 'OXA' impregnation solution provoked a marked increase in the Al/Si ratio found in the liquid phase. In other words, during impregnation, Al atoms are preferentially dissolved from the solid. For the purpose of comparison, the same experiment was realized on the impregnation juice obtained after impregnation with AHM. It is noticeable that such Al-enrichment of the liquid phase is also detected, although to a much lower extend.

The C 1s XPS peak of the OXA10 catalyst before calcination (after drying) is different from the reference AHM catalysts (supplementary information Fig. S2). The latter presents a typical C peak related to classical C contamination, with mainly one intense component at 284.8 eV corresponding to the carbon atoms linked to other C atoms or to H atoms (C–(C, H)). The former shows an intense component at 289.6 eV corresponding to C atoms doubly linked to oxygen (C=O and O–C–O). This signal must be correlated with the presence of the oxalate moieties. Note that after calcination at 400 °C, all samples exhibited a C 1s XPS peak with the classical shape of usual C contamination (not shown), indicating that the oxalate moieties were effectively removed after calcination at 400 °C.

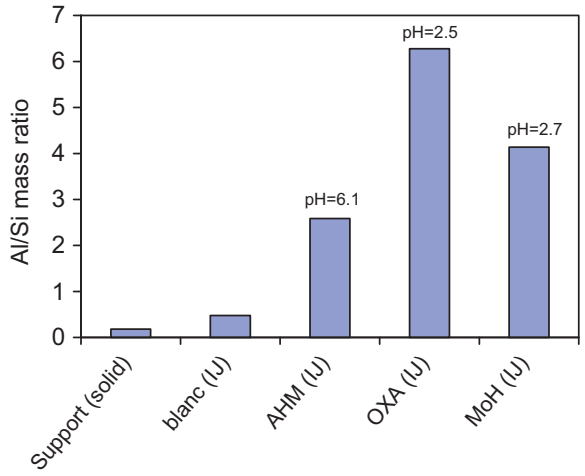

Fig. 6. Al/Si mass ratio determined by ICP-AES on the solid fresh support, A (solid) and on the impregnation juices (IJ) sampled after 2 h of impregnation of the support and 10 min rest with water (A0), AHM (AHM), AHM-oxalate (OXA) and molybdenum oxide hydrates (MoH). The pH of the impregnation solutions was calculated from the pH measured in the precursor solutions and taking the dilution factors into account.

The same samples (before calcination) were analyzed by Raman spectroscopy (Supplementary information Fig. S3). Both AHM and OXA dried samples exhibit a main Raman band at ca. 945 cm^{-1}, attributable to polymolybdate species like heptamolybdate. In the AHM catalyst, the second weak band appears at 896 cm^{-1}, exactly like in heptamolybdate (ν_{as} MoO_{2t} vibration). This band is not clearly visible in the OXA sample.

3.1.2. Metathesis activity

The metathesis activity was measured during one hour on stream for each catalyst. After a short latency stage, a maximum in activity is observed after about 20 min time-on-stream followed by slow deactivation. This behaviour was already described for similar catalysts tested under identical conditions [9,14]. To allow comparisons between catalysts, the specific activity averaged between 14 and 26 min time-on-stream is discussed for each sample. Fig. 7 shows the metathesis specific activity of OXA catalysts, along with previously published [17] results concerning reference AHM catalysts, for the purpose of comparison. It is remarkable that the curve of activity as a function of the loading is increasing in an almost

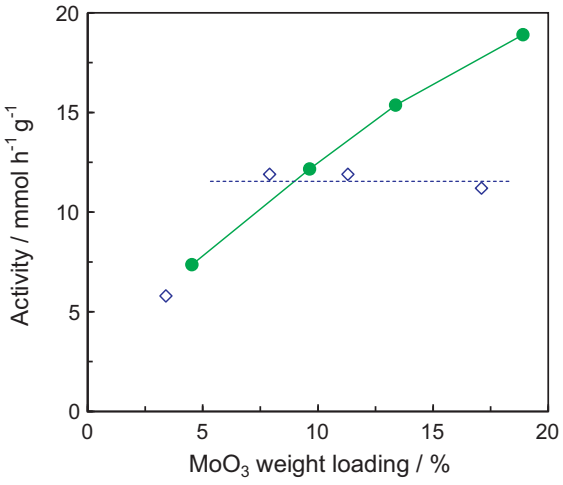

Fig. 7. Specific metathesis activity of (●) OXAx catalysts and comparison with (◊) AHMx400 catalysts [17]. The dotted line is a guide to the eye representing the limit reached with AHM catalysts in terms of activity.

linear way. This is different from the situation encountered with AHM catalysts, for which a plateau was observed for MoO_3 loadings higher than 7 wt.% [17]. A horizontal line at ca. 12 mmol h^{-1} g^{-1} appears as a limit of activity that can be reached with the catalysts prepared with AHM as precursor and calcined at 400 °C (AHM*x*400) [17]. This corresponds to a conversion of about 12% with a selectivity of ca. 99%. At low Mo loading, OXA and AHM*x*400 catalysts exhibit similar performances. At relatively high Mo loading OXA catalysts clearly outperform the AHM catalysts. In other words, the addition of oxalic acid in the impregnation step has a clear positive effect.

3.1.3. Discussion

3.1.3.1. Effect of oxalic acid on the Mo speciation. Unlike the case of the impregnation with AHM (pH = 5.4 for the precursor solution), the pH of the impregnation solutions for OXA catalysts were low. Depending on the targeted loading, an appropriate volume of the precursor solution (pH = 1.8) was diluted in water to reach 200 ml of impregnation solution. The support was thus suspended in an impregnation solution whose pH ranged from 2.1 to 2.8 when the nominal loading was 19 and 5 wt.%, respectively.

The composition of impregnation solutions can be calculated, if the pH and the equilibrium constants are known [29]. In the case of our reference AHM catalysts, equation (1) has to be considered. At the beginning of the wet impregnation the pH ranges from 5.8 to 6.5 after dilution to 200 ml, depending on the targeted loading and mainly MoO_4^{2-} species are present (see supplementary information, Table S1). But during vacuum drying, the concentration of Mo species increases and the equilibrium is shifted (to the right), leading to the deposition of heptamolybdate anions on the support. These 7-Mo atom clusters were identified as a possible reason for the poor dispersion of the Mo oxide phase in catalysts prepared via wet impregnation of AHM (nucleation centres for sintering to MoO_3).

$$7MoO_4^{2-} + 8H^+ \leftrightarrows Mo_7O_{24}^{6-} + 4H_2O \quad (1)$$

Here, oxalic acid was added in the impregnation solution with the hope that it would stabilize – by complexation – different Mo species with lower nuclearity. This strategy can appear surprising, as it is well-known that acidic conditions favour the formation of polymeric species, while isolated molybdates (MoO_4^{2-}) are classically observed under alkaline conditions. Considering the pH effect only, the calculations suggest that $H_2Mo_7O_{24}^{4-}$ and $Mo_8O_{26}^{4-}$ would be the main species, along with $H_3Mo_7O_{24}^{3-}$, $HMo_7O_{24}^{5-}$ and $HMo_8O_{26}^{3-}$ (Table S1). The situation is however not as simple, since additional chemical equilibrium have to be considered to account for the reaction between Mo species and oxalate ligands. The identification of the complexes formed is not straightforward and, to the best our knowledge, the constants for these equations are not available in literature. Ng et al. [55] reported Raman spectra of molybdenum oxalate in solution as a function of the pH and highlighted the stabilization of monomeric molybdodioxalate (pH > 4.25) and dimeric molybdooxalate (1.25 < pH < 4.25). At pH = 2, two most intense peaks were found at 938 cm^{-1} and at 901 cm^{-1}. Such signal is not observed in our precursor solution. Since the higher frequency of the Mo=O stretch indicates an increase in the polymerization degree, it must be concluded that species with nuclearity >2 are obtained here. Note that Ng et al. prepared their solution from molybdenum oxalate salts [55] and not from AHM, so different equilibra were probably reached in their study and in ours. Following Himeno et al. [56], the sharp band at 949 cm^{-1} could be interpreted as the major Raman line of $Mo_3O_{10}^{2-}$ species. However, in such case, other bands at 918 and 901 cm^{-1} should be also present (which is not the case here). Under very acidic conditions species with higher nuclearity are often observed [56]. Here, $Mo_8O_{26}^{4-}$ species (971 and 963 cm^{-1}) are however not detected. Finally, the main Raman features of the OXA-solution (Fig. 1) are very close to the typical bands related to AHM and was not compatible with any of the envisaged species. It thus appears that the heptamolybdate clusters were preserved in the initial precursor solution. It must be stressed, however that all equilibra actually change continuously during vacuum drying, which makes challenging the experimental or predictive identification of the actual deposited species.

After impregnation, the bands observed in the precursor solution can still be distinguished, although much less resolved. In view of the large width of the bands observed for solid-state measurement, it is difficult to discriminate between different supported polyoxomolybdate species. Most of the species indeed consist in edge-sharing octahedra with distorted geometry that give rise to Mo–O vibrations in the same region [57]. In any case, polymeric species, close to heptamolybdate are deposited on the support, as attested by the main Raman signal at ca. 945 cm^{-1} (Fig. S3).

3.1.3.2. Effect of oxalic acid on the support. Characterization results point out the partial dissolution of the support during impregnation in the presence of oxalic acid. Firstly, the Al/Si ratio measured in the liquid phase after the 2 h of stirring is strikingly high (Fig. 6). This observation, related to the low pH of the solution, is consistent with the dissolution of aluminic domains of the support. It is well-known that silica is very resistant against acidic media while alumina already dissolves around pH 4 [58]. The dissolution of alumina support must often be envisaged during catalyst preparation [58,59]. In addition to the simple effect of the acidity of the impregnation medium, the effect of the oxalate ions must be envisaged here. Carrier et al. [60] have highlighted the works of geochemists who reported that oxalate ions enhance the dissolution rate of alumina [61]. This effect has been reported in the case of aluminosilicate clays, for example [62]. It proceeds via the modification of the thermodynamic equilibrium between species in solution. The solubility of aluminium oxide is enhanced because oxalate–aluminium complexes form, thereby shifting the dissolution equilibrium.

Secondly, the texture of the support has been strongly affected by the impregnation procedure (Table 1 and Fig. 2). The pore volume and the mean pore size diameter both decreased drastically in the case of the impregnation in the presence of oxalic acid. These observations contrast with the case of AHM catalysts for which the porosity was barely affected after impregnation [9,14]. Here, large pores seem to collapse, while a population of new very small pores is created during the impregnation. These small pores may either really be formed from the partial dissolution of the support or originate from the partial plugging of bigger pores.

Evidently, the environment of Al atoms has changed drastically after OXA-impregnation. The complexation of Al^{3+} ions by oxomolybdate species must be envisaged. Such effect is known to promote the dissolution of the alumina-containing support [60]. Bergwerff et al. [35] have observed this effect during the preparation of MoO_3/Al_2O_3 extrudates and described it as a chain reaction: Al^{3+} ions generated by the dissolution of the support are consumed during the formation of $Al(OH)_6Mo_6O_{18}^{3-}$, which can precipitate in the form of $(NH_4)_3Al(OH)_6Mo_6O_{18}$ (equation (2)). Since the Al^{3+} concentration is kept low, increasing amounts of aluminium oxide are dissolved. This phenomenon was called to explain the formation of [$AlMo_6$] during the impregnation of the support with AHM [9]. However, no [$AlMo_6$] was detected on the OXA catalyst after impregnation (before calcination) by ^{27}Al MAS-NMR (Fig. 5). So the dissolution of the support is not linked to the complexing effect of oxomolybdates in the present case. Instead, it has to be correlated with the combination of two parameters: (i) the low pH and (ii) the presence of oxalate ligands. Actually, the affinity of dissolved Al^{3+} cations for oxalate ligands appears stronger than their affinity for

oxomolybdenum species.

$$6MoO_4^{2-} + Al^{3+} + 6H^+ \leftrightharpoons Al(OH)_6Mo_6O_{18}^{-3} \quad (2)$$

3.1.3.3. Catalysts properties. After the wet step, no hexamolybdoaluminate ([$AlMo_6$]) was detected by ^{27}Al MAS-NMR. However, [$AlMo_6$] is present in the calcined catalysts (Fig. 5). Note that NMR analyses have been performed on aged samples and that rehydration after calcination can have occurred during storage and manipulations in air. The formation of [$AlMo_6$] via hydration of MoO_3/SiO_2–Al_2O_3 catalyst under ambient humid condition at room temperature is not surprising [14,57].

Comparing AHM and OXA catalysts, another important difference concerns the aluminium molybdate phase. $Al_2(MoO_4)_3$ was clearly detected on the AHM8400 sample and its formation was shown to increase with increasing loading [9]. In the case of the catalysts prepared from the 'OXA' solution, $Al_2(MoO_4)_3$ is not detected except as traces in the catalyst with the highest loading. It appears that, in the absence of [$AlMo_6$] after impregnation, the formation of $Al_2(MoO_4)_3$ during calcination is hampered.

The impregnation with the OXA solution followed by calcination at 400 °C led to a totally amorphous Mo oxide deposit, as confirmed both by Raman and XRD (Fig. 3 and Fig. S1). The fact that no MoO_3 crystals are found in such MoO_3/SiO_2–Al_2O_3 catalysts is a major difference with respect to the classical preparation method based on AHM. This effect can be explained as follows. As demonstrated by Bergwerff et al. [29], the organic ligands (here oxalate) increase the solubility of Mo, thereby preventing its rapid precipitation at the external surface of the support particles. This results in a homogeneous Mo deposit on the available support surface. As Mo species are well dispersed they are less prone to sinter. An additional reason for the absence of MoO_3 is the fact that the formation of $Al(OH)_6Mo_6O_{18}^{3-}$ was avoided during the wet impregnation in the presence of oxalic acid whereas it is known that [$AlMo_6$] yields MoO_3 upon calcination [29,63]. It could be claimed also that the oxalate ligands indirectly impede the agglomeration of Mo species by acting as steric spacers during the adsorption on the support. Finally, another possible factor explaining the absence of MoO_3 crystals concerns the dissolution of the support. Dissolved Al^{3+} ions, possibly complexed by oxalate ligands, will return to the solid state during water evaporation. These species also might play the role of "spacers" or "diluting agents" during the formation of the Mo phase and limit the possibility for pure oxomolybdenum species to agglomerate close to each other and to sinter under the effect of calcination.

3.1.3.4. Correlation with metathesis activity. OXA catalysts have a metathesis activity in the same order or higher than AHM catalysts (Fig. 7). At low MoO_3 loading, they have approximately the same activity as the catalysts prepared by impregnation with the classical AHM solution and calcined at 400 °C. Remarkably however, the metathesis activity rises continuously when the loading increases. This trend differs from the trend typically observed with MoO_3/SiO_2–Al_2O_3 metathesis catalysts (levelling off or drop in activity upon loading increase). In the end, OXA catalysts with relatively high Mo loading (>8–9 wt.% MoO_3) perform better than the corresponding AHM catalysts. It must be remembered also that the specific surface area of the OXA catalysts is negatively affected by the presence of oxalic acid. On a surface basis (activity normalized by the SSA), OXA catalysts are always more active than AHM catalysts.

In AHM catalysts, MoO_3 crystals (XRD and Raman) and $Al_2(MoO_4)_3$ (NMR) were shown to build up when the activity was levelling off [9]. In the present case, the metathesis activity keeps increasing when neither MoO_3 nor $Al_2(MoO_4)_3$ appear in detectable amounts. In other words, the absence of MoO_3 crystals and of aluminium molybdate in the whole range of loading can be correlated with the continuous increase in activity. To be accurate, traces of $Al_2(MoO_4)_3$ are observed on OXA19. At this level the slope of the activity-loading curve gets slightly smaller.

In the end, the control of the nature of the Mo species in solution at the molecular scale was not achieved. Nevertheless, the use of oxalic acid allowed us to prevent the formation of MoO_3 crystals and of aluminium molybdate, which leads to a linear relationship between the specific activity and the MoO_3 loading. Finally, the specific activity of OXA19 (18.9 mmol g^{-1} h^{-1}) is significantly higher than the activity reached with catalysts prepared via the conventional impregnation with AHM.

3.2. Molybdenum oxide hydrates (MoH)

3.2.1. Catalyst characterization

The initial molybdenum oxide hydrates solution was obtained by reaction of metallic Mo with an aqueous solution of hydrogen peroxide followed by catalytic removal of the peroxide in excess. The pH of this yellow solution was 2.0. Fig. 1 shows its Raman spectrum. Two bands are detected at 946 and 967 cm^{-1}. These bands may be attributed to $Mo_3O_{10}^{2-}$ and $Mo_8O_{26}^{4-}$ species respectively [56]. Noticeably, no band was detected in the 848–856 cm^{-1} range, where the vibration modes of side-bonded peroxo ligands are usually expected [64,65]. It indicates that the peroxide species have efficiently been removed catalytically by the treatment with the platinum grid.

For these catalysts the effect of the calcination temperature (300 °C, 400 °C and 500 °C) has been investigated. Also, the loading has been varied in the 5–20 wt.% range for the 400 °C and 500 °C-calcined samples. The experimental MoO_3 loading mostly fits the targeted one or is slightly lower than expected (Table 2). Such discrepancies are attributed to the incomplete recuperation of the Mo that is projected on the walls of the flask during the reaction of metallic Mo and H_2O_2 (these droplets are tentatively recovered during the preparation but some are lost). The filtration is another step of the preparation that can cause losses of Mo (adsorbed on the filter).

Catalysts having similar loading and being calcined at different temperature have very similar texture as shown by similar SSA, pore volume and average pore diameter (Table 2). This is further confirmed by the overlaid pore size distribution curves shown in Fig. 8A for 10%-loaded samples. Catalysts having different MoO_3 loading mainly differ in terms of specific surface area and pore volume: both decrease with increasing loading (Table 2). The mean pore size remains quite stable or decreases slightly. The shapes of the pore size distribution profiles are slightly affected by Mo loading (Fig. 8B). The pore size distribution curves of MoH catalysts tend to shift downwards (with respect to the Y axis) upon addition of Mo oxide.

Investigations were conducted on the impregnation juice and on the dried (but not calcined) catalysts. Fig. 6 shows that in this case also the liquid phase, being in contact with the support during 2 h impregnation, is enriched in Al. The effect is more marked than in the case of impregnation with AHM but less marked than in the case of the OXA solution.

At the surface of the uncalcined catalyst, XPS reveals the usual carbon contamination peak, as no organic compound was used in the preparation (supplementary information, Fig. S2). The Raman spectra of the uncalcined catalysts barely reveal a broad and poorly resolved peak around 958 cm^{-1} (Fig. S3). This frequency may correspond to polyoxomolybdenum species with higher nuclearity than heptamolybdate, e.g. $Mo_8O_{26}^{4-}$.

XRD investigations showed without ambiguity that all MoH samples are amorphous. No MoO_3 crystallites were detected even for the catalysts with the highest loading and calcined

Table 2
Textural properties (N_2-physisorption) and experimental MoO_3 weight loading (ICP-AES) of the MoH catalysts.

Name	Calcination temperature (°C)	MoO_3 loading (wt.%)	SSA ($m^2\,g^{-1}$)	Pore volume ($ml\,g^{-1}$)	Pore diameter (nm)
Support	500	–	490	0.71	5.8
MoH10300	300	9.3	380	0.51	5.4
MoH5400	400	5.0	430	0.59	5.5
MoH10400	400	9.3	390	0.54	5.6
MoH14400	400	12.9	370	0.52	5.6
MoH20400	400	20.3	330	0.46	5.6
MoH5500	500	4.6	390	0.57	5.8
MoH10500	500	9.5	370	0.51	5.5
MoH14500	500	12.9	320	0.47	5.9
MoH20500	500	18.8	290	0.43	6.0

at the highest temperature (see supplementary information, Fig. S4 and S5).

In the same way, Raman spectra showed no bands related to the presence of MoO_3 crystals (Fig. 9). Instead a broad band around 950 cm^{-1} is detected. It is attributed to surface polymolybdates [48]. In some cases (like MoH14400) a shoulder at ~990 cm^{-1} was detected. Consistently, Hinokuma et al., reported that the condensation of such peroxopolyanions gives large chain-shaped polyanions based corner-sharing [MoO_5OH] octahedral which were characterized by Raman bands at 950 and 980 cm^{-1} [39]. Bearing in mind that Raman measurements were very delicate (in line with the fluorescence of the support and with the low response of amorphous species) and considering the large width of the Raman bands discussed, it will be considered that the band at 950 cm^{-1}, sometimes accompanied by a shoulder at 990 cm^{-1}, is associated to a stoichiometrically ill-defined amorphous surface polymolybdates.

The Mo surface concentration measured in XPS increases linearly with increasing MoO_3 loading (Fig. 4). Unlike AHM catalysts [9], the surface Mo/(Si + Al) atomic ratio is always lower than the bulk Mo/(Si + Al) atomic ratio. In addition, in MoH catalysts, the calcination temperature has no marked effect on the surface Mo/(Si + Al) atomic ratio.

The ^{27}Al-MAS NMR spectra show that after impregnation of the support with the MoH solution, the environment of Al atoms is affected (Fig. 10). Mainly the Al_{PEN} (ca. 30 ppm) and Al_{TET} (ca. 54 ppm) components of the spectra decrease. In MoH10 catalysts, a small amount of [$AlMo_6$] (15 ppm) is detected after impregnation. After calcination at 300 °C, 400 °C or 500 °C, the Al_{TET} signal is restored and the signal of [$AlMo_6$] increases slightly. After calcination at 500 °C, traces of $Al_2(MoO_4)_3$ are detected at −14 ppm. In the catalysts calcined at 400 °C, the [$AlMo_6$] species (15 ppm) is always present (Fig. 11A). Its signal intensity does not increase proportionally with increasing loading. $Al_2(MoO_4)_3$ (−14 ppm) appears only at high loading (traces in MoH14400) and its signal is intense only in the MoH20400 catalyst. Similarly, in the catalysts calcined

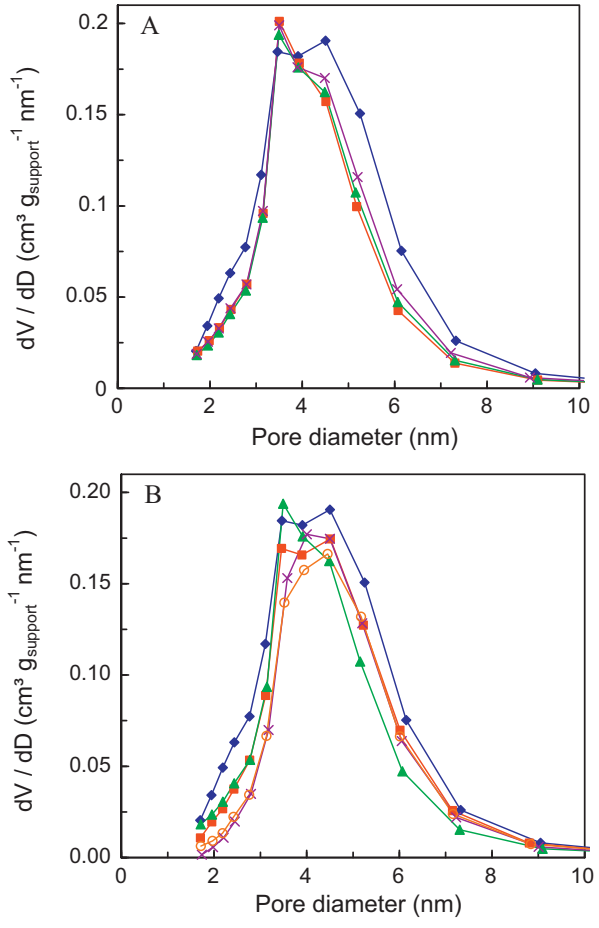

Fig. 8. Pore size distribution determined by the BJH method applied on the desorption isotherms of (◆) the support and MoH catalysts. Graph A: (■) MoH10300, (×) MoH10400 and (▲) MoH10500. Graph B: (■) MoH5500, (▲) MoH10500, (×) MoH14500 and (○) MoH20500.

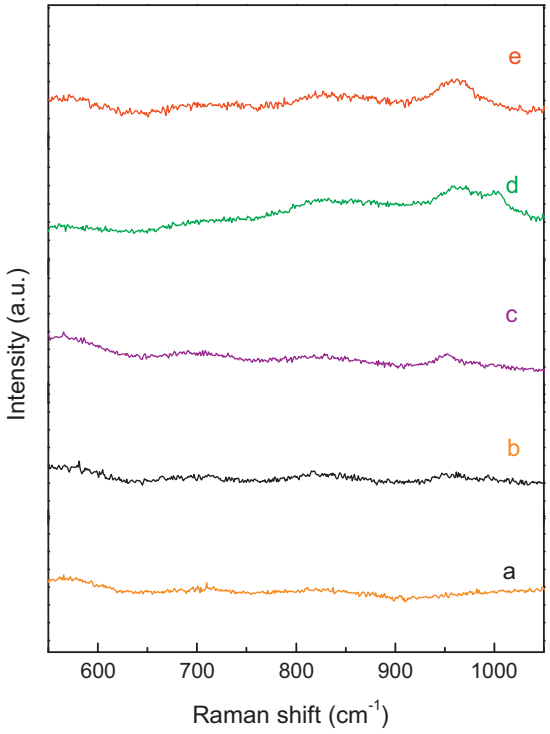

Fig. 9. Raman spectra of (a) the SiO_2–Al_2O_3 support, (b) MoH5400, (c) MoH10400, (d) MoH14400 and (e) MoH20400.

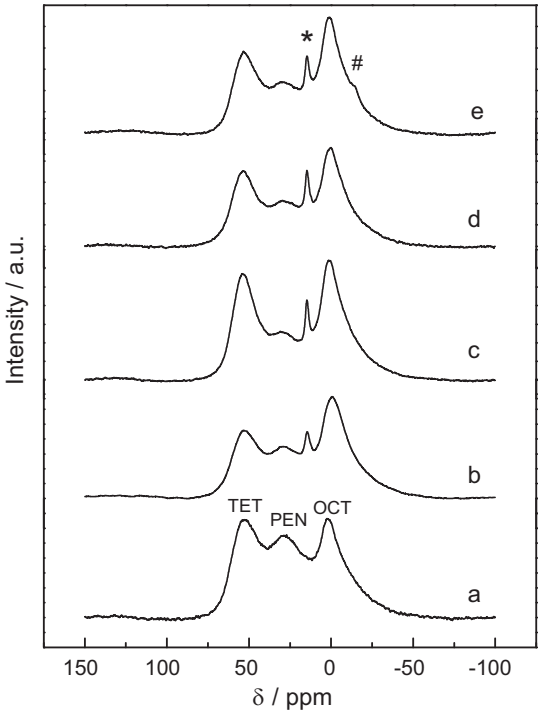

Fig. 10. ^{27}Al MAS-NMR spectra of (a) the support, (b) MoH10 dried but not calcined, (c) MoH10300, (d) MoH10400 and (e) MoH10500. The Al_{TET}, Al_{PEN} and Al_{OCT} signals are indicated on the first spectrum. [$AlMo_6$] and $Al_2(MoO_4)_3$ are marked with "*" and "#" respectively.

at 500 °C, the [$AlMo_6$] species is always present (Fig. 11B). Its intensity does not vary in parallel with the MoO_3 loading. Traces of $Al_2(MoO_4)_3$ already appear at relatively low loading even if this signal remains feeble up to 14 wt.% in MoO_3. In MoH20500 the aluminium molybdate phase is even more abundant than in MoH20400.

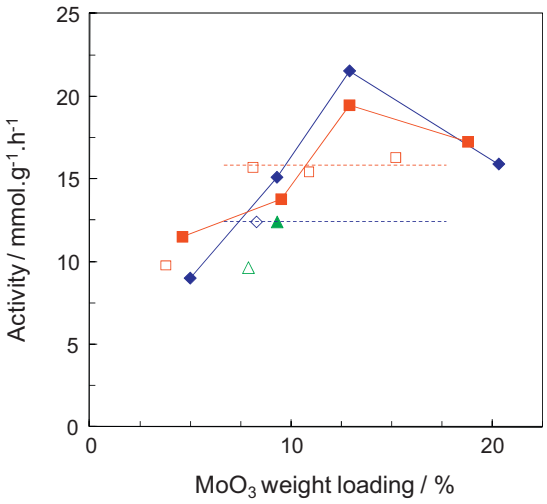

Fig. 12. Specific activity of MoH*x* catalysts. (▲) MoH10300, (◆) MoH*x*400 and (■) MoH*x*500. For comparison, the activity is also given for AHM*xy* catalysts: (△) AHM8300, (◇) AHM8400 and (□) AHM*x*500. Horizontal dotted lines are guides to the eye indicating the plateau observed in the activity of AHM catalysts as described in [9].

3.2.2. *Metathesis activity*

The activity of MoH catalysts develops with time on stream in a similar way as already depicted for AHM [9,17] and OXA catalysts. The activity of the 10 wt.% loaded catalysts was slightly dependent on the calcination temperature (Fig. 12). The 400 °C-treated sample is the most active, followed by the catalysts calcined at 500 °C and finally by the one, calcined at 300 °C.

The highest activity is reached with MoH14400 (ca. 22 mmol g^{-1} h^{-1}). Overall, the relationship between the metathesis activity and the MoO_3 loading is different from the trends depicted in the case of AHM or OXA catalysts. Here, the activity first increases steeply when the loading is increased up to 14 wt.%. Then a marked decrease is observed. While MoH14400 and MoH14500 catalysts are much more active than AHM catalysts

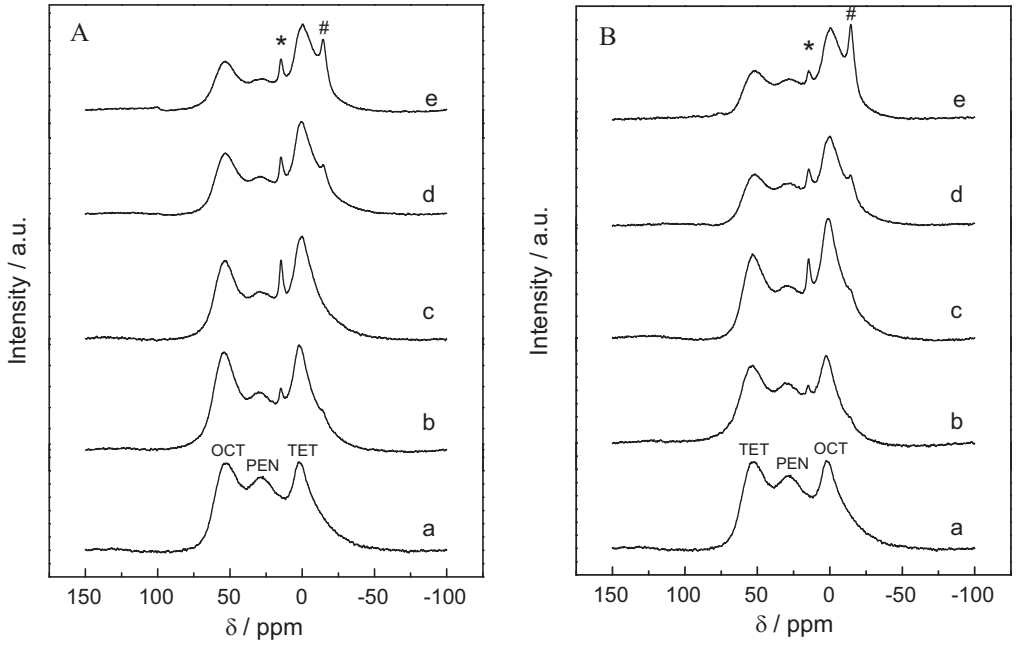

Fig. 11. (A) ^{27}Al MAS-NMR spectra of (a) the support, (b) MoH5400, (c) MoH10400, (d) MoH14400 and (e) MoH20400. The Al_{TET}, Al_{PEN} and Al_{OCT} signals are indicated on the first spectrum. (B) ^{27}Al MAS-NMR spectra of (a) the support, (b) MoH5500, (c) MoH10500, (d) MoH14500 and (e) MoH20500. The Al_{TET}, Al_{PEN} and Al_{OCT} signals are indicated on the first spectrum. [$AlMo_6$] and $Al_2(MoO_4)_3$ are marked with "*" and "#" respectively.

with corresponding loading and calcination temperature, the activity of the 20 wt.% loaded catalysts falls down around the plateau of activity described earlier for AHM*x*500 catalysts.

3.2.3. Discussion

3.2.3.1. Mo speciation in the molybdenum oxide hydrates solution. It is clear that the molybdenum species in the MoH impregnation solution are different from those found in the AHM or OXA ones (Fig. 1). The peak at 950 cm^{-1} could be attributed to the trimolybdate anion ($Mo_3O_{10}^{2-}$) following Himeno et al. [56]. However, the presence of the trimolybdate species remains uncertain since the $Mo_8O_{26}^{4-}$ species, clearly revealed by the peak at 967 cm^{-1}, also generate a peak around 950 cm^{-1} [48,56]. The presence of species with nuclearity higher than eight, like $Mo_{36}O_{112}^{8-}$ (main Raman signal expected at 983 cm^{-1}) is also possible as their signal would fall in the high frequency shoulder of the 967 cm^{-1} peak. In any case, as the most intense Raman signals are found at higher frequencies, species with a higher condensation degree than 7 are present.

3.2.3.2. Effect of the MoH solution on the support. As the solution is very acidic (almost as acidic as the 'OXA' solution), partial dissolution of the support was expected. Indeed, the Al/Si ratio measured by ICP-AES in the impregnation juice was relatively high (Fig. 6). A ligand-promoted dissolution can be envisaged under the effect of oxomolybdenum species, that would lead to the formation of the [$AlMo_6$] species, as observed in the case of MoO_3/Al_2O_3 catalysts preparation [60]. Indeed, this species is observed in MAS-NMR after the impregnation (Fig. 10).

Here, the porosity of the support is moderately affected by the preparation. The specific surface area and the pore volume decrease more than in the case of impregnation with AHM (Table 2). The mean pore size diameter tends to decrease slightly after impregnation. In addition, Fig. 8 shows that this is not a simple effect of the addition of non-porous MoO_3 but that the porosity of the support itself is clearly affected. Overall, it must be concluded that the MoO_x phase enters the pores. In parallel, the Al_{TET} and Al_{PEN} signals are only slightly reduced after impregnation, unlike in the case of impregnation with the Mo-oxalate solution. This confirms that the drastic alteration of the support described in the previous section was promoted by oxalic acid, while here the sole effect of the acidity of the solution is not enough to provoke a considerable dissolution of the support.

3.2.3.3. Catalysts properties. All MoH catalysts were totally amorphous. The calcination temperature has no effect on the crystallinity of the catalysts, unlike in the case of AHM catalysts where the calcination at 400 °C and 500 °C provoked the appearance of MoO_3 crystals. This can appear surprising because the species found in the impregnation solution are also polymeric species and could thus also act as potential nucleation points for Mo oxide sintering. However, rational explanations can be put forward to explain such result.

Firstly, as discussed above, the Mo species are thought to enter the pores of the support instead of precipitating mainly at the outer surface of the particles, like in the case of AHM catalysts. This is suggested both by textural analysis and by the determination of the low Mo surface concentration by XPS, particularly at high Mo loading. Mo atoms that are located inside the porosity of the particles will not be detected by XPS. It should be remembered that the tentative formula of the species formed in solution via the oxidation of Mo by the hydrogen peroxide solution is $MoO_3 \cdot nH_2O \cdot mH_2O_2$ (with m presumably close to 0 after the treatment with the Pt grid). It is reasonable to put forward that such species interact less with the positively charged support surface than the heptamolybdate anions. Indeed if present as anionic species in a very acidic solution, the Mo entities should be more protonated than the heptamolybdate cluster under moderate pH. So during the impregnation with the MoH solution, the Mo species have a better chance to be transported on the whole available surface, including the interior of the porosity. Mo species (even polymeric species with high nuclearity) that are well dispersed on the whole available surface have a lower probability to agglomerate and sinter.

The second plausible explanation to account for the absence of MoO_3 crystals concerns [$AlMo_6$]. It is known that hexamolybdoaluminium yields crystalline MoO_3 (and aluminium molybdate) upon calcination [9,29,63]. Here, this species is detected by Al-MAS NMR in the dried catalyst (Fig. 10) but in much lower quantities than in AHM catalysts.

The calcination temperature determines whether $Al_2(MoO_4)_3$ forms or not. In fact among the 10 wt.% loaded samples, only the catalyst treated at 500 °C exhibits traces of this aluminium molybdate phase. Formation of $Al_2(MoO_4)_3$ is further favoured when the loading increases. It seems that, above a certain limit in terms of MoO_3 loading, the formation of high amounts of aluminium molybdate cannot be avoided. This transition occurs clearly when the MoO_3 loading increases from 14 to 20 wt.%. If MoH*x*400 and MoH*x*500 samples are compared to AHM*x*500 catalysts [9] the following observations can be made about the $Al_2(MoO_4)_3$ signal at −14 ppm: (i) at 4–5 wt.% loading, only traces of $Al_2(MoO_4)_3$ (if any) are detected regardless of the preparation method (ii) at 8–10 and 11–14 wt.% loading a clear peak is detected for AHM catalysts, while only traces are detected in MoH samples and (iii) at high loading (17–20 wt.%) all catalysts exhibit a significant amount of $Al_2(MoO_4)_3$. This shows that the preparation of MoO_3/SiO_2–Al_2O_3 catalysts via the impregnation of molybdenum oxide hydrates solution impedes the formation of $Al_2(MoO_4)_3$ at intermediate loading.

3.2.3.4. Correlation with metathesis activity. Increasing the calcination temperature of AHM8 catalysts resulted in a marked increase of activity. Here, the calcination temperature of the MoH10 catalysts has a smaller impact. Interestingly however, the 400 °C-treated sample is the most active. No discrimination can be made between the three MoH10 catalysts on the basis of their texture, their surface composition (XPS) or their crystallinity (XRD, Raman). In MAS-NMR, the intensity of the [$AlMo_6$] species is similar. Traces of $Al_2(MoO_4)_3$ are detected in the catalyst calcined at 500 °C, while this species is not detected at all in the catalyst calcined at 400 °C. So aluminium molybdate can tentatively be pointed out as responsible for the slightly lower activity of the MoH10500 catalyst.

The dependence of the metathesis activity of MoH catalysts as a function of the MoO_3 loading is different from the relationship established for AHM and OXA catalysts. A marked increase in activity is observed when the loading rises up to ca. 14 wt.%. The superior activity of MoH catalysts in the range of intermediate loading (8–14 wt.%) can be interpreted in relationship with physico-chemical characterization data. Firstly, MoH10 and MoH14 catalysts are totally amorphous even when the calcination is carried out at high temperature while AHM8500 and AHM11500 exhibit MoO_3 crystals [9]. Exactly like in the case of OXA catalysts, the activity increases linearly with the loading as long as no MoO_3 crystals form. Secondly, $Al_2(MoO_4)_3$ was also clearly present in AHM8500 and AHM11500, as witnessed by a NMR peak at −14 ppm [9]. In the case of MoH10 and MoH14 catalysts, this peak is either absent or barely detectable (Fig. 11). Again, the presence of aluminium molybdate appears detrimental.

Similar interpretation can be developed to explain why the activity of MoH catalysts suddenly drops when the MoO_3 loading is set to 20 wt.% (MoH20400 and MoH20500). This loading corresponds to an abrupt increase in the intensity of the peak at −14 ppm. In fact the amount of $Al_2(MoO_4)_3$ in MoH20400 and

MoH20500 appears similar to the amount detected in AHM15500 which itself is a modest metathesis performer.

4. Conclusions

Two Mo precursors have been investigated as alternatives to the most classical ammonium heptamolybdate precursor for impregnating silica alumina. In the first case, oxalic acid was added to a solution of ammonium heptamolybdate. The second precursor solution was obtained by oxidation of metallic Mo with a hydrogen peroxide solution. The catalysts were characterized at different stages of their preparation and their metathesis activity was measured. It is interesting to keep in mind that all catalysts undergo thermal activation before the reaction. The latter step can again affect their physico-chemical properties (as interestingly studied by Stoyanova et al. via in situ techniques [66]). Nevertheless, the present study demonstrates that the "preparation history" of the catalysts has a strong impact on their final performance.

The presence of oxalic acid apparently did not lead to the stabilization of oxomolybdenum species with low nuclearity. Instead, the heptamolybdate clusters appears to be preserved. The solution of molybdenum oxide hydrates contains polymeric species like $Mo_8O_{26}^{4-}$ and the presence of species with even higher nuclearity is plausible.

Both investigated precursor solutions are very acidic, which has an impact on the support. Partial dissolution of the support during the impregnation step has been evidenced. In the presence of oxalate ligands, the dissolution is more pronounced because of the formation of Al-oxalate complexes. As a result, the texture of the samples obtained via impregnation in the presence of oxalic acid is significantly affected.

Unlike catalysts prepared via the impregnation of AHM, the samples obtained via the alternative precursors are totally amorphous whatever their loading and calcination temperature. In the presence of oxalic acid, stable Al-oxalate complexes are formed which prevents the formation of $[AlMo_6]$ and the rapid precipitation of Mo anions at the outer surface of the support particles. In the case of the impregnation with the molybdenum oxide hydrates solution, Mo atoms appear to be better dispersed down to the bottom of the pores (as compared to impregnation with AHM). In parallel, the formation of $[AlMo_6]$ is low. In both cases, the improved dispersion of Mo species on the whole available surface of the support hampers their sintering to MoO_3 crystals.

Aluminium molybdate was formed to a lesser extent in the catalysts prepared via the alternative precursors as compared to the reference AHM precursor. This is explained by the fact that lower amount (if any) of $[AlMo_6]$ is formed during impregnation with the OXA or the MoH solutions.

In the end, the metathesis activity reached with OXA catalysts is in the same order (low Mo loading) or higher (high Mo loading) than the activity obtained with catalysts prepared via impregnation of AHM and calcined at the same temperature. The activity increases linearly with the MoO_3 loading. This trend is put in parallel with the absence of crystalline MoO_3 and $Al_2(MoO_4)_3$ on the whole range of loading inspected. This further recognizes the latter species as detrimental for the development of a high metathesis activity.

MoH catalysts with intermediate loading are significantly more active than AHM catalysts. These best catalysts present the combination of favourable factors: the texture of the support is not strongly affected, there is no MoO_3 and only traces of $Al_2(MoO_4)_3$ (if any) are detected. At 20 wt.% loading, the specific activity drops and this phenomenon is correlated with the abrupt production of aluminium molybdate.

Acknowledgments

Guy Daelen is acknowledged for having performed the NMR experiment. Prof. B.-L. Su and Dr. A. Léonard are thanked for the access to the NMR facilities (FUNDP, Namur). Martin Holena is acknowledged for the calculations of impregnation solution compositions. D.P. Debecker thanks the FNRS for his Research Fellow position and UMICORE for the 2010 Scientific Award. The authors from UCL are involved in the "Inanomat" IUAP network sustained by the Service public fédéral de programmation politique scientifique (Belgium), in the Cost Action D41 sustained by the European Science Foundation and in the European Multifunctional Material Institute (EMMI) built on the basis of the former "FAME" Network of Excellence of the EU 6th FP.

Appendix A. Supplementary data

Supplementary data associated with this article can be found, in the online version, at doi:10.1016/j.molcata.2011.03.011.

References

[1] J.A. Chodorge, C. Dupraz, Patent: FR2880018 (2006).
[2] H. Fritzm, Patent: DE102006039904 (2008).
[3] R.J. Gartside, M.I. Greene, Patent: WO2005009929 (2005).
[4] P. Schwab, B. Breitscheidel, C. Oost, R. Schulz, M. Schulz, Patent: US2002197190(A1) (2002).
[5] J.C. Mol, J. Mol. Catal. A 213 (2004) 39–45.
[6] X. Zhu, X. Li, S. Xie, S. Liu, G. Xu, W. Xin, S. Huang, L. Xu, Catal. Surv. Asia 13 (2009) 1–8.
[7] H. Liu, L. Zhang, X. Li, S. Huang, S. Liu, W. Xin, S. Xie, L. Xu, J. Nat. Gas Chem. 18 (2009) 331–336.
[8] D. Lokhat, M. Starzak, M. Stelmachowski, Appl. Catal. A 351 (2008) 137–147.
[9] D.P. Debecker, M. Stoyanova, U. Rodemerck, A. Leonard, B.-L. Su, E.M. Gaigneaux, Catal. Today, doi:10.1016/j.cattod.2010.07.026.
[10] K. Zama, Y. Imada, A. Fukuoka, M. Ichikawa, Appl. Catal. A 194–195 (2000) 285–296.
[11] A. Salameh, A. Baudouin, D. Soulivong, V. Boehm, M. Roeper, J.-M. Basset, C. Copéret, J. Catal. 253 (2008) 180–190.
[12] A. Behr, U. Schüller, K. Bauer, D. Maschmeyer, K.D. Wiese, F. Nierlich, Appl. Catal. A 357 (2009) 34–41.
[13] H. Balcar, D. Mishra, E. Marceau, X. Carrier, N. Zilková, Z. Bastl, Appl. Catal. A 359 (2009) 129–135.
[14] D.P. Debecker, M. Stoyanova, U. Rodemerck, P. Eloy, A. Léonard, B.-L. Su, E.M. Gaigneaux, J. Phys. Chem. C 114 (2010) 18664–18673.
[15] D.P. Debecker, M. Stoyanova, U. Rodemerck, E.M. Gaigneaux, Stud. Surf. Sci. Catal. 175 (2010) 581–585.
[16] J. Handzlik, J. Ogonowski, J. Stoch, M. Mikolajczyk, P. Michorczyk, Appl. Catal. A 312 (2006) 213–219.
[17] D.P. Debecker, K. Bouchmella, C. Poleunis, P. Eloy, P. Bertrand, E.M. Gaigneaux, P.H. Mutin, Chem. Mater. 21 (2009) 2817–2824.
[18] D.P. Debecker, B. Schimmoeller, M. Stoyanova, C. Poleunis, P. Bertrand, U. Rodemerck, E.M. Gaigneaux, J. Catal. 277 (2011) 154–163.
[19] H. Balcar, J. Čejka, in: Y. İmamoğlu, V. Dragutan (Eds.), Metathesis Chemistry: From Nanostructure Design to Synthesis of Advanced Materials, Springer, 2007, pp. 151–166.
[20] D.P. Debecker, D. Hauwaert, M. Stoyanova, A. Barkschat, U. Rodemerck, E.M. Gaigneaux, Appl. Catal. A 391 (2011) 78–85.
[21] X. Li, W. Zhang, S. Liu, X. Han, L. Xu, X. Bao, J. Mol. Catal. A 250 (2006) 94–99.
[22] X. Li, A.M. Zheng, J. Guan, X.W. Han, W.P. Zhang, X.H. Bao, Catal. Lett. 138 (2010) 116–123.
[23] T. Ookoshi, M. Onaka, Chem. Commun. (1998) 2399–2400.
[24] J. Guan, G. Yang, D.H. Zhou, W.P. Zhang, X.C. Liu, X.W. Han, X.H. Bao, J. Mol. Catal. A 300 (2009) 41–47.
[25] J. Handzlik, J. Mol. Catal. A 316 (2010) 106–111.
[26] M.N. Kwini, J.M. Botha, Appl. Catal. A 280 (2005) 199–208.
[27] X.J. Li, W.P. Zhang, X. Li, S.L. Liu, H.J. Huang, X.W. Han, L.Y. Xu, X.H. Bao, J. Phys. Chem. C 113 (2009) 8228–8233.
[28] J. Handzlik, J. Stoch, J. Ogonowski, M. Mikolajczyk, J. Mol. Catal. A 157 (2000) 237–243.
[29] J.A. Bergwerff, T. Visser, B.R.G. Leliveld, B.D. Rossenaar, K.P. de Jong, B.M. Weckhuysen, J. Am. Chem. Soc. 126 (2004) 14548–14556.
[30] A. Beltrán, F. Caturla, A. Cervilla, J. Beltrán, J. Inorg. Nucl. Chem. 43 (1981) 3277–3282.
[31] D. Navez, G. Weinberg, G. Mestl, P. Ruiz, E.M. Gaigneaux, Stud. Surf. Sci. Catal. 143 (2002) 609–617.
[32] A. Klisinska, A.-S. Mamede, E.M. Gaigneaux, Thin Solid Films 516 (2008) 2904–2912.
[33] F. Bertinchamps, C. Gregoire, E.M. Gaigneaux, Appl. Catal. B 66 (2006) 10–22.

[34] D.P. Debecker, F. Bertinchamps, N. Blangenois, P. Eloy, E.M. Gaigneaux, Appl. Catal. B 74 (2007) 223–232.
[35] J.A. Bergwerff, M. Jansen, B.G. Leliveld, T. Visser, K.P. de Jong, B.M. Weckhuysen, J. Catal. 243 (2006) 292–302.
[36] T.N. Aridi, M.A. Al-Daous, Appl. Catal. A 359 (2009) 180–187.
[37] A. Klisinska, A.S. Mamede, E.M. Gaigneaux, Catal. Today 128 (2007) 145–152.
[38] A. Maione, M. Devillers, J. Solid State Chem. 177 (2004) 2339–2349.
[39] K. Hinokuma, K. Ogasawara, A. Kishimoto, S. Takano, T. Kudo, Solid State Ionics 53–6 (1992) 507–512.
[40] E.M. Gaigneaux, K.-I. Fukui, Y. Iwasawa, Thin Solid Films 374 (2000) 49–58.
[41] E.R. Braithwaite, J. Haber, Molybdenum: An Outline of Its Chemistry and Uses, Elsevier, Amsterdam, 1994, p. 662.
[42] P.C. Bakala, E. Briot, J.Y. Piquemal, J.M. Bregeault, P. Beaunier, Catal. Commun. 8 (2007) 1447–1451.
[43] P.C. Bakala, E. Briot, L. Salles, J.M. Bregeault, Appl. Catal. A 300 (2006) 91–99.
[44] J.-M. Brégeault, M. Vennat, S. Laurent, J.-Y. Piquemal, Y. Mahha, E. Briot, P.C. Bakala, A. Atlamsani, R. Thouvenot, J. Mol. Catal. A 250 (2006) 177–189.
[45] U. Rodemerck, P. Ignaszewski, M. Lucas, P. Claus, Chem. Eng. Technol. 23 (2000) 413–416.
[46] O. Collart, P. Van der Voort, E.F. Vansant, E. Gustin, A. Bouwen, D. Schoemaker, R.R. Rao, B.M. Weckhuysen, R.A. Schoonheydt, Phys. Chem. Chem. Phys. 1 (1999) 4099–4104.
[47] A.N. Desikan, L. Huang, S.T. Oyama, J. Phys. Chem. 95 (1991) 10050–10056.
[48] G. Mestl, T.K.K. Srinivasan, Cat. Rev.: Sci. Eng. 40 (1998) 451–570.
[49] T. Ono, M. Anpo, Y. Kubokawa, J. Phys. Chem. 90 (1986) 4780–4784.
[50] H. Jeziorowski, H. Knozinger, P. Grange, P. Gajardo, J. Phys. Chem. 84 (1980) 1825–1829.
[51] E.J.M. Hensen, D.G. Poduval, P.C.M.M. Magusin, A.E. Coumans, J.A.R. van Veen, J. Catal. 269 (2010) 201–218.
[52] K.J.D. MacKenzie, J. Temuujin, K. Okada, Thermochim. Acta 327 (1999) 103–108.
[53] P. Cloos, A.J. Leonard, J.P. Moreau, A. Herbillon, J.J. Fripiat, Clays Clay Miner. 17 (1969) 279–287.
[54] T.-H. Chen, K. Houthoofd, P.J. Grobet, Microporous Mesoporous Mater. 86 (2005) 31–37.
[55] K.Y.S. Ng, X. Zhou, E. Gulari, J. Phys. Chem. 89 (1985) 2477–2481.
[56] S. Himeno, H. Niiya, T. Ueda, Bull. Chem. Soc. Jpn. 70 (1997) 631–637.
[57] X. Carrier, E. Marceau, M. Che, Pure Appl. Chem. 78 (2006) 1039–1055.
[58] J.P. Brunelle, Pure Appl. Chem. 50 (1978) 1211–1229.
[59] E. Baumgarten, F.O. Geldsetzer, U. Kirchhausen-Düsing, J. Colloid Interface Sci. 173 (1995) 104–111.
[60] X. Carrier, J.F. Lambert, M. Che, J. Am. Chem. Soc. 119 (1997) 10137–10146.
[61] W. Stumm, Chemistry of the Solid–Water Interface: Process at the Mineral–Water Interface and Particle–Water Interface in Natural Systems, J.W. Sons, New York, 1992, pp. 165–169.
[62] R.W. Smith, Coord. Chem. Rev. 149 (1996) 81–93.
[63] X. Carrier, M. Che, Appl. Catal. A 253 (2003) 317–320.
[64] D. Bayot, M. Devillers, D. Peeters, Eur. J. Inorg. Chem. (2005) 4118–4123.
[65] D. Bayot, B. Tinant, M. Devillers, Inorg. Chim. Acta 357 (2004) 809–816.
[66] M. Stoyanova, U. Rodemerck, U. Bentrup, U. Dingerdissen, D. Linke, R.W. Mayer, H.G.J. Lansink Rotgerink, T. Tacke, Appl. Catal. A 340 (2008) 242–249.